INSTITUTE OF PHYSICS PUBLISHING CLASSICAL AND QUANTUM GRAVITY

Class. Quantum Grav. **18** (2001) 2543–2550 www.iop.org/Journals/cq PII: S0264-9381(01)25302-7

STEP error model development

P Worden, J Mester and R Torii

Hansen Experimental Physics Laboratory, Stanford University, Stanford, California, 94305, USA

Received 1 April 2001

Abstract

We describe the ongoing development of a comprehensive error model for the satellite test of the equivalence principle, STEP. The goal is to employ a model of the experiment and apparatus as a self-consistent whole. The model uses a set of input parameters based on experiment design and the measured characteristics of STEP sensor systems. The output of the model evaluates specific disturbances to the test masses in the general categories of thermal noise, gas pressure forces, electrical forces, magnetic forces, gravitational forces, radiation pressure and vibration. Use of the model to set experiment requirements and to evaluate design trade-offs are briefly discussed.

PACS number: 0480C

(Some figures in this article are in colour only in the electronic version; see www.iop.org)

Introduction

The goal of the satellite test of the equivalence principle, STEP, is to test the apparent equivalence of gravitational and inertial mass to 1 part in 10^{18} (Lockerbie *et al* 2000, Mester *et al* 2001). This represents an increase of greater than five orders of magnitude over ground-based experiments and lunar laser-ranging observations (Adelberger 1994, Su *et al* 1994, Williams *et al* 1996). In an experiment of this sensitivity, a comprehensive error model is essential for understanding and setting requirements and evaluating design trade-offs. In the following we describe the development of a comprehensive error model program and describe its application to the development of the STEP experiment.

The goal of the STEP error model is to embody a model of the experiment and apparatus (especially including trade-offs) as a self-consistent whole. The program systematically evaluates the known errors starting from a relatively small and consistent set of assumptions, and because it efficiently and explicitly incorporates the major trade-offs, it can be used to set experiment requirements. Many experimental parameters, which in previous studies were considered independent, are in fact explicitly dependent on other parameters or requirements. The program automatically calculates these, for example signal frequency from orbit height and satellite spin rate or less directly the minimum common mode rejection ratio from the setup currents and coil dimensions in the SQUID position sensor. This feature prevents much of the inconsistency that results from independent assumptions and independent analyses of individual experiment systems.

Error model program design

To maintain consistency and uniformity of treatment of the various error sources, we have implemented our current understanding of the experiment in a single computer program with a unified database and assumptions. The starting point for this program is the STEP error analysis, a text document actively maintained on our server for use in trade studies. The STEP error analysis derives analytic estimates of specific disturbances to the masses in the general categories of thermal noise, gas pressure forces, electrical forces, magnetic forces, gravitational forces, radiation pressure and vibration. It also includes estimates of disturbances to the measurement system, including measurement noise, changes to the superconductors and thermal and mechanical stability. The next level of analysis, typically done in a higher-level language such as Mathematica, uses results from the STEP error analysis and other documents to produce detailed analytic solutions for the response of the accelerometers, drag-free system or noise sources. These solutions are pasted into the final error analysis program.

In effect the error analysis program calculates the spectral response of the entire system. This approach is more efficient in determining the desired results (i.e. the noise spectral density at signal frequency) than simulating the time development would be and is no more subject to the usual errors in assumptions and interpretation than a full simulation. The error analysis program is implemented in a spreadsheet with each cell corresponding to a unique input variable, such as a dimension of a test mass, or an output calculated from prior inputs, such as the position sensitivity of a SQUID sensor (calculated from currents and inductance values). The spreadsheet structure makes interactions and dependencies explicit and traceable, so that the analysis is to that extent self-documenting. Documentation for the derivation of formulae is maintained in the higher-level languages from which the solutions are pasted, so that only comments and references need to be maintained in the error analysis program itself.

Examples of the specific disturbances considered include electric potentials in the housing surrounding the mass (including patch effect), the radiometer effect, losses from eddy current damping, gravitational coupling from helium tide, drag-free residual vibration coupled to the differential mode, SQUID noise, penetration depth changes in superconductors and momentum transfer from penetrating particle radiation.

Error model input

The error model incorporates a large set of input parameters falling in the following categories: natural parameters, including the Earth's gravity field, magnetic field, atmospheric drag and South Atlantic anomaly, cosmic ray and solar flare radiation fluxes; instrument parameters including test mass properties, sensor coil electrode and bearing gap spacings, niobium film emissivity and penetration depth temperature coefficients, spacecraft geometry, magnetic and radiation shielding factors and instrument thermal contractions; experiment parameters including temperature and thermal gradients, ambient pressure, orbit altitude and eccentricity and spacecraft rotation rate and stability; and a wide range of systems parameters such as SQUID sensor white noise, $1/f$ knee, temperature coefficients and inductance, sensor coil geometry factors, magnetic bearing geometry and setup currents, electrostatic positioning system and charge control parameters and drag-free control law parameters and thruster noise.

Where possible, these input parameters and derived models are based on actual measurements of systems that will be used for STEP or are derived from established electrical and mechanical properties of materials to be used in the fabrication of the STEP instrument, taking account of the particular baseline instrument design. For example, the STEP accelerometer detection system will use SQUIDs that were developed and flight qualified for

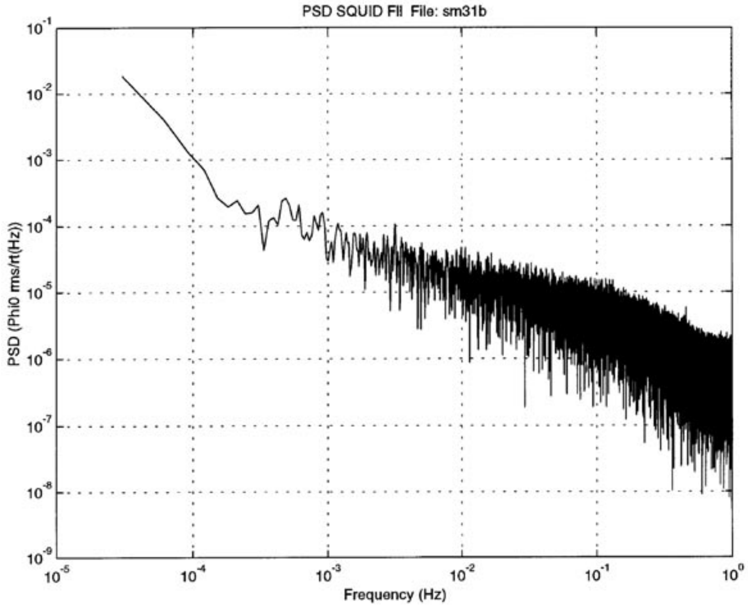

Figure 1. GP-B SQUID noise spectrum. EP signal frequency range is approximately 1.7×10^{-4} – 8×10^{-4} Hz.

the Gravity Probe B Relativity Mission. We use measurements of the noise spectral density of the GP-B SQUIDs, in the frequency range relevant to STEP, to model the expected SQUID noise. The measured flux noise characteristic of a typical GP-B SQUID is shown in figure 1. The error model uses an analytic approximation to the measured noise energy of the SQUID, characterized by $1/f$ behaviour at low frequency (< 0.1 Hz) and a constant power spectral density at higher frequency. The circuit connected to the SQUID converts the power spectral density to an equivalent flux noise per root Hz (and may add additional noise of its own). In the error model, the approximation to the SQUID noise is used as input to the solution for the position sensor circuit, to give the expected flux noise (and sensor resolution). This output becomes input for models of other STEP systems.

Error model results

The ultimate output of the error analysis program is an estimate for the performance of the experiment. Figure 2(a) depicts error model program results for a particular set of input parameters, a few of which are listed at the bottom of the table, such as the position sensor gap (the nominal spacing between test mass and SQUID sensor coils), the spacecraft roll rate, and orbit altitude. The common mode period and differential mode period are outputs that the program calculates for the given set of input parameters including gap spacing, mass ratios of the test mass pair and sensor coil inductance and currents. The program determines the proper sensor coil current ratios to achieve good common mode balance, i.e. a large common mode rejection ratio. For each disturbance, a systematic component at signal frequency is calculated and the output is given as an effective differential acceleration. Error sources which are known to be incoherent, e.g. thermal noise, are converted to an expectation value at the signal frequency by RMS averaging. Coherent errors (e.g. temperature driven effects, helium

(*a*)

DFC Reference accelerometer Disturbance	Systematic component at signal frequency m/sec^2	Comment
SQUID noise	2.37E-18	acceleration equivalent to intrinsic noise
SQUID temp. drift	9.52E-19	regulation of SQUID carriers
Thermal expansion	8.11E-19	gradient along DAC structure
Differential Thermal expansion	5.08E-23	Radial gradient in DAC structure
Nyquist Noise	8.56E-19	RMS acceleration equivalent
Gas Streaming	3.44E-19	decaying Gas flow, outgassing
Radiometer Effect	9.01E-19	gradient along DAC structure
Thermal radiation on mass	1.87E-22	Radiation pressure, gradient
Var. Discharge uv light	3.45E-19	unstable source, opposite angles on masses
Earth field leakage to SQUID	1.06E-18	estimate for signal frequency component
Earth Field force	1.40E-22	estimate for signal frequency component
Penetration depth change	3.31E-20	longitudinal gradient
Electric Charge	3.03E-19	Assumptions about rate *
Electric Potential	6.42E-19	variations in measurement voltage
Sense voltage offset	5.62E-19	bias offset
Drag free residual in diff. Mode	3.92E-20	estimated from squid noise
Viscous coupling	3.37E-24	gas drag + damping
Cosmic ray momentum	3.36E-21	mostly directed downward
Proton radiation momentum	2.33E-18	unidirectional, downward
dynamic CM offset	9.87E-19	vibration about setpoint, converted **
static CM offset limit	3.02E-20	A/D saturation by 2nd harmonic gg
Trapped flux drift acceleration	7.38E-23	actual force from Internal field stability
Trapped flux changes in squid	3.54E-19	apparent motion from internal field stability
S/C gradient + CM offset	1.99E-32	gravity gradient coupling to DFC residual of S/C
rotation stability	4.84E-20	centrifugal force variation + offset from axis

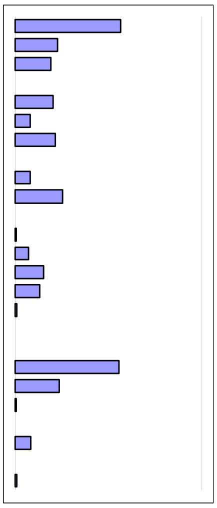

position sensor gap, mm	1.00	500000	Orbit height
common mode period	1474	0.0086	Sensor current, A
differential mode period	1135	2.6E-10	CM distance, m
S/C rotation per orbit	- 2.72E+00		
Total error	**1.30E-17**	**RMS error** **4.18E-18**	m/sec^2

(*b*)

DFC Reference accelerometer Disturbance	Systematic component at signal frequency m/sec^2	Comment
SQUID noise	2.31E-18	acceleration equivalent to intrinsic noise
SQUID temp. drift	9.41E-19	regulation of SQUID carriers
Thermal expansion	8.02E-19	gradient along DAC structure
Differential Thermal expansion	5.08E-23	Radial gradient in DAC structure
Nyquist Noise	8.62E-19	RMS acceleration equivalent
Gas Streaming	3.39E-19	decaying Gas flow, outgassing
Radiometer Effect	9.07E-19	gradient along DAC structure
Thermal radiation on mass	1.88E-22	Radiation pressure, gradient
Var. Discharge uv light	3.48E-19	unstable source, opposite angles on masses
Earth field leakage to SQUID	1.05E-18	estimate for signal frequency component
Earth Field force	1.40E-22	estimate for signal frequency component
Penetration depth change	3.29E-20	longitudinal gradient
Electric Charge	4.43E-19	Assumptions about rate *
Electric Potential	6.46E-19	variations in measurement voltage
Sense voltage offset	1.53E-19	bias offset
Drag free residual in diff. Mode	2.16E-19	estimated from squid noise
Viscous coupling	1.79E-23	gas drag + damping
Cosmic ray momentum	3.39E-21	mostly directed downward
Proton radiation momentum	6.50E-19	unidirectional, downward
dynamic CM offset	5.53E-18	vibration about setpoint, converted **
static CM offset limit	1.70E-19	A/D saturation by 2nd harmonic gg
Trapped flux drift acceleration	7.43E-23	actual force from Internal field stability
Trapped flux changes in squid	3.50E-19	apparent motion from internal field stability
S/C gradient + CM offset	5.62E-31	gravity gradient coupling to DFC residual of S/C
rotation stability	2.70E-19	centrifugal force variation + offset from axis

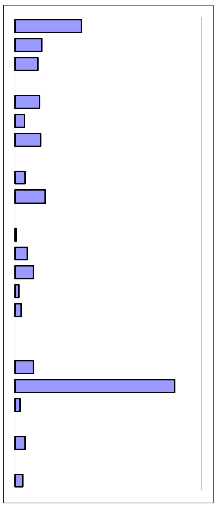

position sensor gap, mm	1.00	400000	Orbit height
common mode period	1486	0.0086	Sensor current, A
differential mode period	1142	1.4E-09	CM distance, m
S/C rotation per orbit	- 2.72E+00		
Total error	**1.60E-17**	**RMS error** **6.46E-18**	m/sec^2

Figure 2. Typical errors for (*a*) a 500 km orbit and (*b*) a 400 km orbit.

tide) are calculated at signal frequency. These errors are treated two ways. Since it is not possible in most cases to determine the phase difference between independent error sources, the errors are summed as if they all had the same phase. This gives a worst case estimate for the total error. For a statistical estimate, the errors are summed in an RMS sense. Our requirements are chosen using the worst case sum.

Figures 2(*a*) and (*b*) show illustrative results for different orbit heights, 500 and 400 km respectively, with no other changes. Some differences are readily apparent. Vibrations of the test masses about their equilibrium positions result in changing centre of mass offsets that can couple gravity gradients into the signal frequency. The vibrations are caused by residual satellite motion, and we call this disturbance the '*dynamic CM offset*'. It is greatly increased at the lower altitude relative to the other disturbances. The drag-free residual in the differential mode of the accelerometers (*drag-free residual in differential mode*) is a direct limitation to how well the masses remain centred, and this residual is increased by the overall increase in drag in the lower orbit. Consequently the centring system cannot work so well in a lower orbit, and the disturbance increases rapidly with the centring error. There is a similar cause for the smaller increase in the disturbance from electrical charge. The charge control system's performance (*electric charge*) is also determined by the overall drag-free residual, so that the charge cannot be measured or controlled so well in a low orbit. This overwhelms the expectation that the charging problem would be less because the radiation decreases in lower orbits. The smallest charge that can be measured depends on the residual acceleration noise from drag, and the charge cannot be controlled better than it can be measured. In the model used for the radiation flux and its interaction with the test masses, the increase in drag is larger than the decrease in the disturbing flux, within the range of likely altitudes for STEP. These two examples illustrate the utility of an integrated model of the full system in setting experiment requirements such as orbit altitude.

Certain clusters of variables, for example the SQUID sensitivities and spring constants resulting from the SQUID setup, couple to most or all of the errors. These variables represent states of the 'machine' which converts accelerations into an equivalence principle measurement. This 'machine' comprises the mathematical model of the accelerometers and satellite together with their interactions. Some insight into the relative importance of disturbances to the experiment can be gained by studying these clusters.

In the example of figure 1, the leading disturbance is given in the row labelled SQUID noise. This is the acceleration equivalent to the sensor noise of the SQUID. In a less integrated calculation, estimates would be made for only the factors directly leading to the disturbance: SQUID noise at signal frequency, differential acceleration sensitivity, observation time, etc. The STEP error model program instead calculates some of these (SQUID noise at signal frequency, differential acceleration sensitivity) from prior assumptions. In particular, inductance values and their derivatives are calculated from test mass dimensions, and spring constants from inductance values and the setup currents, all of which go into the differential acceleration sensitivity. There is therefore no possibility of picking a differential acceleration sensitivity that is inconsistent with the basic assumptions about the apparatus. This prevents inconsistency of the sort which would arise, for example, from changing assumptions about the spacecraft rotation (which would not normally be included as having any effect on the SQUID noise disturbance). Centrifugal force is a significant contribution to the total spring constant and, consequently, changing the satellite rotation changes the differential acceleration sensitivity. The differential acceleration sensitivity determines the scale factor for conversion of the $1/f$ noise of the SQUID to acceleration.

Sensor noise, more than any other disturbance, is the largest single disturbance to STEP. This gives a limitation to the performance of the accelerometer and ultimately to the drag-free control and other systems as well. Thus, because the drag-free control can never do better than the sensor limit and because several disturbances (including gravity-gradient noise and the performance of the charge measurement system) depend in turn on the performance of the drag-free control, it is extremely important to use the best possible sensor for the input to the drag-free control.

Additional disturbances

Details of the treatment of several highly visible disturbances are discussed below. Generically, most disturbances are calculated individually for each test mass. Where appropriate, the disturbance is calculated as a function of frequency and the power spectral density at the signal frequency is the disturbance to the experiment. These disturbing forces are inputs to the model of the accelerometer. The model calculates the response of the accelerometer to the disturbance. The differential mode acceleration at signal frequency contains any equivalence principle information and the common mode acceleration becomes the input to the model of the drag-free system.

Dynamic centre of mass offset

The centre of mass offset couples to gravity gradients, producing a disturbance proportional to the product of the gradient and the offset. The largest gravity gradients that are harmonically related to the equivalence principal signal are those from the Earth. These are not a direct concern, so long as the centre of mass offset is constant, because they have twice the frequency of the signal and can be distinguished from it. Our ability to make this distinction is modelled by the *static centre of mass offset*. But if the centre of mass offset is time dependent, a component of the gravity-gradient disturbance will in general appear at the signal frequency. This disturbance we say is due to the *dynamic centre of mass offset*.

The test masses are constrained radially by the magnetic bearing system with a period ω_{r}, which is nominally 60 seconds. The oscillations of the masses are excited principally by residual spacecraft motion $\mathrm{DFC}(\omega)$ which has a broad spectrum and which is itself the response of the drag-free control system to drag variations and sensor noise. Damping is provided by the electrostatic positioning system and the drag-free control system. Under the assumption of linearity (almost always valid in STEP) the amplitude of the masses' motion at any frequency is the product of the residual force from the spacecraft and the harmonic oscillator response $H(\omega, \omega_{\mathrm{r}})$ of the test masses; that is, the centre of mass offset $\Delta x(\omega) = \int(\omega' - \omega, \omega_{\mathrm{r}})^{*}\mathrm{DFC}(\omega')^{*}\omega'^{2}\mathrm{d}\omega'$. In turn, this amplitude, multiplied by the gravity gradient, gives the dynamic centre of mass disturbance: $\delta a = \int x(\omega' - \omega)^{*} g'(\omega')\mathrm{d}\omega'$. A major simplification comes from the fact that the gravity gradient has essentially a line spectrum, so that the integrals need only be evaluated in a narrow bandwidth around specific frequencies. Two frequencies are of major concern, the signal frequency itself and three times the signal frequency. The difference between these and the gravity gradient (at twice signal frequency) is equal to the signal frequency. The disturbance amplitudes at these two frequencies are very likely correlated, so the calculation simply adds them for a worst-case estimate.

Proton and cosmic ray momentum

Energetic particles that stop in the test masses deposit both energy and momentum, which is not entirely negligible on the scale of forces we are measuring. Given the radiation flux, energy and direction, it is straightforward to make simple estimates of the shielding factors and absorption of the particles in the test masses. The characteristics of the radiation itself are the biggest uncertainty in this calculation. The radiation is highly variable in space, time and direction; it is particularly difficult to predict over the polar regions. The proton flux from the radiation belts is modelled by a purely empirical fit to published data, which is said to be variable by a factor of more than two. This model captures the major dependencies of the flux intensity and energy in the range of likely STEP orbits, but not elsewhere. The angular distribution of the radiation is not known and was assumed to be entirely downward. This is a worst case assumption, since isotropic radiation results in no net force. Cosmic rays are assumed to be uniform around the orbit, but protons are concentrated in the area of the South Atlantic anomaly. To capture the frequency dependence of the proton disturbance, we multiplied the model by an approximation to the spectrum seen by a satellite passing occasionally through a disturbance fixed on a rotating Earth. We attach no particular significance to the numerical value of the result. A proton monitor will enhance our knowledge of the radiation environment on STEP.

Nyquist noise

This is the mechanical equivalent of electrical Nyquist noise, converted to an equivalent acceleration, i.e. the fundamental thermal noise limit of the measurement. The calculation assumes an independent thermal fluctuation force on each mass, which is the input to the accelerometer model. These forces are uncorrelated and therefore are added in an RMS sense to give an estimate of the total disturbance.

Thermal expansion

Disturbances originating in temperature changes enter the measurement in several ways. The most important are apparent motion of the test masses resulting from thermal changes in dimensions and changes in sensitivity of the apparatus. These are minimized by the double-differential design of the accelerometers: the position of each test mass is measured by the difference in inductance of two matched coils and the equivalence measurement is proportional to the difference in two mass positions, scaled so that the response to a common acceleration is zero. These disturbances are therefore proportional to manufacturing and setup errors, which are small. The error analysis estimates the component of thermal change at signal frequency for thermal gradients along the accelerometers and for thermal differences between the inner and outer accelerometers of a set. Since the thermal gradients within a differential accelerometer are likely to be highly correlated, the results are added to give a best estimate of the disturbance.

Conclusion

STEP is necessarily a highly optimized experiment with many design trade-offs. A thorough error analysis is required to perform these trades effectively. Requirements must in many cases be traded against each other and the allowable size of disturbances from all sources must be budgeted, to optimize the performance of the equivalence principle measurement. Because the same controlling variables appear in many places, sections of the error analysis cannot be simply split off and requirements set separately without risking inconsistency. Future work will incorporate improvements in the model of spacecraft dynamics and drag-free control laws now under study (Jafry 1996, Wiegand *et al* 2000). Further measurements of the electrostatic positioning system characteristics and charge control system parameters will also improve the overall model of experiment performance. While the development of the comprehensive error model for STEP is an ongoing effort it has already proved useful in setting requirements and determining design trades.

Acknowledgments

Many contributions to the error model have been made by the International STEP Collaboration. We also gratefully acknowledge support from NASA code U under contract JPL-959723-16.

References

Adelberger E G 1994 Modern tests of the universality of free fall *Class. Quantum Grav.* **11** A9

Jafry Y 1996 Drag-free control for MiniSTEP *Class. Quantum Grav.* **13** A179

Lockerbie N, Mester J, Torii R, Vitale S and Worden P W 2000 STEP: a status report *Proc. Gyros, Clocks and Interferometers: Testing General Relativity in Space (Bad Honnef, Germany, 22–27 August 1999)*

Mester J, Torii R, Worden P, Lockerbie N, Vitale S and Everitt C W F 2001 The STEP mission: principles and baseline design *Class. Quantum Grav.* **18** 2475

Su Y, Heckel B R, Adelberger E G, Gundlach J H, Harris M, Smith G H and Swanson H E 1994 New tests of the universality of free fall *Phys. Rev.* D **50** 3614

Wiegand M *et al* 2000 Personal communication

Williams J G, Newhallm X X and Dickey J O 1996 Relativity parameters determined from lunar laser ranging *Phys. Rev.* D **53** 6730